Ring Dynamics of DL-Proline and DL-Proline Hydrochloride in the Solid State: A ^2H Nuclear Magnetic Resonance Study

Susanta K. Sarkar,[†] P. E. Young,[‡] and D. A. Torchia*[§]

Contribution from the Bone Research Branch, National Institute of Dental Research, National Institutes of Health, Bethesda, Maryland 20892, and the Department of Chemistry, York College, C.U.N.Y., Jamaica, New York 11451. *Received February 20, 1986*

Abstract: We have measured and analyzed ^2H NMR line shapes and spin–lattice relaxation times of polycrystalline samples of DL-[4,4-$^2H_2$]proline and DL-[4,4-$^2H_2$]proline hydrochloride. Analysis of the line shapes using a two-site exchange model shows that, at 20 °C, the root mean square fluctuation in the orientation of each C–^2H bond axis, θ_{rms}, is 29.3° in DL-[4,4-$^2H_2$]proline. The values of θ_{rms} are independent of temperature from 49 to −85 °C. In contrast the correlation times obtained from an analysis of orientation-dependent inversion–recovery spectra are temperature dependent, and an Arrhenius plot yields an apparent activation energy, ΔF, of 1.3 kcal. Below −85 °C, θ_{rms} decreases as temperature decreases, and a nearly ideal "static" Pake powder pattern with ν_Q = 127 kHz is observed at −170 °C. In the case of DL-[4,4-$^2H_2$]proline hydrochloride the apparent activation energy is 0.6 kcal and θ_{rms} is essentially constant, 24 ± 0.5°, from 20 to −130 °C. Within ±5% the values of θ_{rms} and ΔF derived from a restricted diffusion model of motion are the same as those obtained from the exchange model. Analysis of line shapes of DL-[3,3,4,4,5,5-$^2H_6$]proline shows that θ_{rms} equals 22.1°, 29.0°, and 10.8° for the respective β, γ, and δ positions of the proline ring. In the case of the hydrochloride, the values of θ_{rms} are 20.8°, 25.0°, and 13.6° for the β, γ, and δ positions, respectively. The correlation times for the $^2H_6$ compounds at 20 °C were in agreement with the correlation times obtained for the corresponding $^2H_2$ compounds. The values of θ_{rms} and τ obtained in the solid state are compared with values reported in solution studies. Also, the sensitivity of the proline ring motion to packing in the solid state is discussed with reference to obtaining information about packing and ring environments in proteins.

The conformational freedom of the proline residue is restricted because the peptide nitrogen, α carbon, and three side-chain carbons form a pyrrolidone ring.[1] As a result, the proline residue has unusual, though important, conformational preferences.[2] In globular proteins proline is seldom located in α-helical or β-sheet domains because it destabilizes these structures; rather, the proline residue is usually located in bend or loop structures where the polypeptide chain reverses its direction.[2-4] The interest in proline ring structures and dynamics stems, in part, from a desire to understand better the conformational preferences of this amino acid residue.

A survey[5] of X-ray crystal structures of proline and peptides containing proline has shown that many different puckered ring conformations are observed in the solid state; furthermore, the observed conformations are the low-energy conformations computed by using single-bond torsional potentials.[5] In addition to conformational variability, the X-ray work has also demonstrated that the β, γ, and δ ring positions often have large temperature factors. The observation of large temperature factors for these ring carbons in a variety of different crystal structures[6-8] suggests that large temperature factors result from ring motion rather than crystalline disorder. Recently, a correlation between Pro ring carbon temperature factors and ring motion has been demonstrated in the crystalline peptide *cyclo*(Gly-Pro-D-Ala)$_2$.[8,9] ^{13}C NMR[10] relaxation measurements have provided abundant evidence for proline ring flexibility in peptides in solution.[11-16] A careful analysis of these experiments[16] has yielded quantitative estimates of the angular amplitudes of the motions at the various ring positions and has established an upper limit on the correlation time for the ring motion.

Although previous work has provided much information about proline ring dynamics, solid-state ^2H NMR can significantly extend the accuracy and scope of this information. The complicating effects of overall motion are absent in the solid state. Therefore line shapes and relaxation times are directly related to the amplitudes and rates of the ring motions,[17-21] and these quantities can be determined much more straightforwardly than in solution. The molecular environment of one of the molecules studied, DL-proline hydrochloride, is well-defined, because its crystal structure is known.[7] This permits one to examine the effect of intermolecular interactions upon ring dynamics.

[†] Present Address: Department of Radiology, The Johns Hopkins Medical Institutions, Baltimore, Maryland 21205.
[‡] York College.
[§] National Institute of Dental Research.

(1) A preliminary account of a portion of the work reported herein was presented: Sarkar, S. K. 9th American Peptide Symposium, Toronto, Canada, June 23–28, 1985.
(2) Levitt, M. *Biochemistry* **1978**, *17*, 4277–4284.
(3) Chothia, C.; Janin, J. *Proc. Natl. Acad. Sci. U.S.A.* **1978**, *78*, 4146–4150.
(4) Rose, G. D.; Gierasch, L. M.; Smith, J. A. *Adv. Protein Chem.* **1985**, *37*, 1–109.
(5) Madison, V. *Biopolymers* **1977**, *16*, 2671–2692 and references therein.
(6) Leung, Y. C.; Marsh, R. E. Acta Cryst. 1958, *11*, 17.
(7) Mitsui, Y.; Tsuboi, M.; Iitaka, Y. *Acta Crystallogr., Sect. B: Struct. Sci.* **1969**, *B25*, 2182–2192.
(8) Kostansek, E. C.; Lipscomb, W. N.; Thiessen, W. E. *J. Am. Chem. Soc.* **1979**, *101*, 834–836.
(9) Sarkar, S. K.; Torchia, D. A.; Kopple, K. D.; VanderHart, D. L. *J. Am. Chem. Soc.* **1984**, *106*, 3328–3331.
(10) Abbreviations used are as follows: NMR, nuclear magnetic resonance; $^2H_2$-Pro, DL-[4,4-$^2H_2$]proline; $^2H_2$-Pro·HCl, DL-[4,4-$^2H_2$]proline hydrochloride; $^2H_6$-Pro, DL-[3,3,4,4,5,5-$^2H_6$]proline; $^2H_6$-Pro·HCl, DL-[3,3,4,4,5,5-$^2H_6$]proline hydrochloride; t_1, delay time after 180° pulse in inversion–recovery pulse sequence; t_2, delay time after 90° pulse in quadrupole echo pulse sequence; EFG, electric field gradient; ν_s, quadrupole splitting; ν_Q, quadrupole coupling constant; ν_x, ν_y, and ν_z, principal frequencies, bars over frequencies mean motionally averaged values; $\hat{\mu}$, a unit vector along the C–^2H bond axis; $2\Theta_0$, the angle made by $\hat{\mu}_1$ and $\hat{\mu}_2$ in the two-site exchange model; $2\Theta_D$, the angle through which $\hat{\mu}$ diffuses in the restricted diffusion model; θ_{rms}, the root mean square value of θ, calculated assuming that θ is negative when Φ is 270°; τ_e and τ_D, the respective correlation times in the two-site exchange and restricted diffusion models; D, the rotational diffusion constant; T_1, the spin-lattice relaxation time; and ΔF, the apparent activation energy.
(11) Deslauriers, R.; Walter, R.; Smith, I. C. P. *Biochem. Biophys. Res. Commun.* **1973**, *53*, 244.
(12) Torchia, D. A.; Lyerla, J. R., Jr. *Biopolymers* **1974**, *13*, 97.
(13) Komoroski, R. A.; Peat, I. R.; Levy, G. C. *Biochem. Biophys. Res. Commun.* **1975**, *65*, 272.
(14) Fossel, E. T.; Easwaran, K. R. K.; Blout, E. R. *Biopolymers* **1975**, *14*, 927.
(15) Deslauriers, R.; Smith, I. C. P. In *Topics in Carbon-13 NMR Spectroscopy*; Levy, G. C., Ed.; Wiley: New York, 1976; pp 2–80 and references therein.
(16) London, R. E. *J. Am. Chem. Soc.* **1978**, *100*, 2678–2685 and references therein.
(17) Spiess, H. W. *NMR Basic Principles and Progress*; Springer-Verlag: Berlin, 1978; Vol. 11.
(18) Griffin, R. G. *Methods Enzymol.* **1981**, *72*, 108–174.
(19) Torchia, D. A.; Szabo, A. *J. Magn. Reson.* **1982**, *49*, 107–121. The angular dependence in eq 9 differs in appearance from that of eq 37 in this reference because crystal fixed-coordinate systems are oriented differently.
(20) Torchia, D. A. *Annu. Rev. Biophys. Bioeng.* **1984**, *13*, 125–144.

0002-7863/86/1508-6459$01.50/0

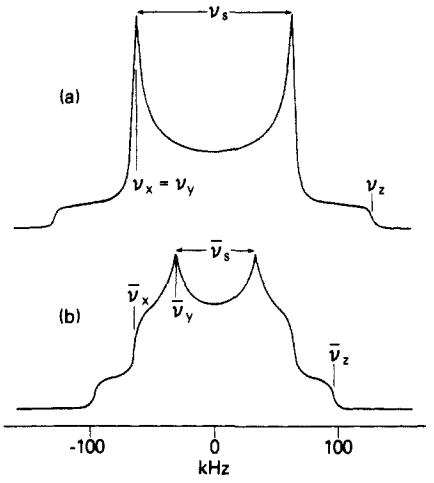

Figure 1. Calculated ^2H NMR powder patterns showing principal frequencies and quadrupole splittings: (a) axially symmetric ($\eta = 0$) Pake pattern expected for a rigid C–^2H bond axis with principal frequencies $\nu_x = \nu_y = -63.75$ kHz and $\nu_z = 127.5$ kHz; (b) axially asymmetric ($\eta = {}^1/_3$) pattern that results when the C–^2H bond axis rapidly jumps between two sites differing in orientation by 48.2°. The motionally averaged principal frequencies $\bar{\nu}_x$, $\bar{\nu}_y$, and $\bar{\nu}_z$ have respective values of −63.75, −31.88, and 95.62 kHz. In case a $\nu_Q = \nu_z = \nu_s$ while in case b $\bar{\nu}_Q = \bar{\nu}_z$ and $\bar{\nu}_s = 2|\bar{\nu}_y|$. Because the EFG tensor has zero trace, the sum of the principal frequencies vanishes in cases a and b.

In addition to enhancing our understanding of the dynamics of the pyrrolidine ring, NMR studies of crystalline proline provide important insights about possible internal motions of the proline residue in proteins.

Experimental Section

$^2H_2$-Pro and $^2H_6$-Pro were synthesized by using the procedure of Young and Torchia.[22] The corresponding hydrochlorides, $^2H_2$-Pro·HCl and $^2H_6$-Pro·HCl, were made by adding a small molar excess of 6 N HCl to aqueous solutions of the parent compounds. Solvent was removed by rotary evaporation. All compounds were crystallized from absolute EtOH and dried over P_2O_5 under vacuum for 24 h. Samples (60–90 mg) were packed into 5-mm NMR tubes and stored in vials containing $CaSO_4$. The samples were stored over a desiccant, because when this was not done, the NMR powder patterns of $^2H_2$-Pro and $^2H_6$-Pro were observed to change with time. These changes were almost certainly due to hydrate formation, since the original (dry) powder spectrum was nearly restored when the samples were vacuum-dried over P_2O_5 for 48 h.

Solid-state ^2H NMR spectra were obtained at 6 T (38.45 MHz) on a home-built spectrometer described previously.[23] Spectra at 12 T (76.77 MHz) were recorded on a NIC-500 spectrometer modified for solid-state work.[24] Deuterium spectra were obtained by using a quadrupole echo pulse sequence[25] $90°_{\pm x}$–t_2–$90°_{y}$–t_2 with a 90° pulse duration of ca. 2 μs and t_2 in the range 20–30 μs. Inversion–recovery spectra were obtained by applying a $180°$–t_1 sequence immediately prior to the quadrupole echo sequence. Depending upon the temperature, from 32 to 512 free-induction decay signals were accumulated in quadrature, with 2048 points per channel. A 2-MHz sampling rate was employed, and a 2-kHz digital line broadening was applied to improve the signal to noise ratio.

Simulations of the spectra were calculated on a DEC-10 computer. The principal frequencies were measured directly from the observed spectra, and fast-limit powder line shapes were then calculated by using the standard formulas for the line shape.[17] The theoretical spectra were convoluted with 2-kHz Lorentzian line broadening, and the values of the principal frequencies listed in the tables were those that yielded the best agreement between measurement and calculated spectra. The inversion–recovery spectra were simulated by calculating the partially relaxed signal intensity for each orientation of B_0 (see Theory section). The rotational correlation time was allowed to vary until the best agreement between theory and experiment was attained. All theoretical spectra, except those in Figure 1, were corrected for finite pulse power of both 180° and 90° pulses, using formulas given by Hiyama et al.[24] and Bloom et al.[26]

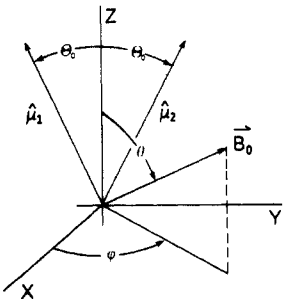

Figure 2. Principal axis system of the ^2H EFG tensor averaged by a rapid exchange of the C–^2H bond axis ($\hat{\mu}$) between two orientations $\hat{\mu}_2$ and μ_1 having equal equilibrium probabilities. The orientations of $\hat{\mu}_2$ and $\hat{\mu}_1$ are defined by polar angles (Θ_0, 90°) and (Θ_0, 270°), respectively. In order to satisfy the convention $|\bar{\nu}_z| \geq |\bar{\nu}_x| \geq |\bar{\nu}_y|$, Θ_0 must be $\leq 35.26°$. The orientation of the external field, B_0, is defined by polar angles (θ, ϕ).

Theory

In this section we briefly summarize the equations that will be used to analyze the ^2H NMR spectra. The orientation-dependent frequency of a quadrupolar nucleus, $I = 1$, in a strong field, B_0, is given by eq 1, where (θ_0, ϕ_0) are the spherical polar angles that

$$\nu = \nu_Q(3\cos^2\theta_0 - 1 - \eta\sin^2\theta_0\cos 2\phi_0)/2 \quad (1)$$

define the orientation of B_0 in the principal axis system of the electric field gradient (EFG) tensor, $4\nu_Q/3$ is the quadrupole coupling constant, e^2qQ/h, and η is the asymmetry parameter. In the case of deuterium bonded to carbon, η is nearly 0, so that to an excellent approximation ν is given by eq 2. For a polycrystalline sample, the spectrum corresponding to eq 2 is a Pake pattern,[27] Figure 1a. Typically, e^2qQ/h is about 170 kHz for ^2H, and therefore ν_Q is about 128 kHz. When $\eta = 0$, ν_s, the quadrupole splitting (the separation of the spectral maxima), equals ν_Q, Figure 1a.

$$\nu = \nu_Q(3\cos^2\theta_0 - 1)/2 \quad (2)$$

Reorientation of the C–^2H bond axis will markedly affect the ^2H line shape[17,27] when $\omega_Q\tau_c \lesssim 1$, where τ_c is the rotational correlation time and $\omega_Q = 2\pi\nu_Q$. In general, the calculation of the line shape must be done on a digital computer. However, the calculation is greatly simplified if the fast-limit condition $\omega_Q\tau_c \ll 1$, is satisfied. In this case, the motionally averaged orientation-dependent frequency is given by eq 3, where (θ, ϕ) are the

$$\bar{\nu} = \bar{\nu}_Q(3\cos^2\theta - 1 - \bar{\eta}\sin^2\theta\cos 2\phi)/2 \quad (3)$$

polar angles that define the orientation of B_0 in the averaged EFG principal axis system and $\bar{\nu}_Q$ and $\bar{\eta}$ are the motionally averaged values of ν_Q and η. Figure 2 illustrates the orientation of the averaged EFG principal axis system in the case of rapid exchange of the C–^2H bond axis[28,29] between two orientations (Θ, Φ) = (Θ_0, 90°) and (Θ, Φ) = (Θ_0, 270°) having equal equilibrium probability.

(21) Spiess, H. W. *Adv. Polym. Sci.* **1985**, *66*, 442.
(22) Young, P. E.; Torchia, D. A. In *Peptides: Structure and Function*; Hruby, V. J., Rich, D. H., Eds.; Pierce: Rockford, IL, 1983; pp 155–158.
(23) Sarkar, S. K.; Sullivan, C. E.; Torchia, D. A. *J. Biol. Chem.* **1983**, *258*, 9762–9767.
(24) Hiyama, Y.; Silverton, J. V.; Torchia, D. A.; Hammond, S. J.; Gerig, J. T. *J. Am. Chem. Soc.* **1986**, *108*, 2715–2723.
(25) Davis, J. H.; Jeffery, K. R.; Bloom, M.; Valic, M. I.; Higgs, T. P. *Chem. Phys. Lett.* **1976**, *42*, 390–394.
(26) Bloom, M.; Davis, J. H.; Valic, M. I. *Can. J. Phys.* **1980**, *58*, 1510–1517.
(27) Abragam, A. *The Principles of Nuclear Magnetism*; Oxford: London, 1961.
(28) Soda, G.; Chiba, T. *J. Chem. Phys.* **1969**, *50*, 439–455.
(29) Jelinski, L. W.; Sullivan, C. E.; Batchelder, L. S.; Torchia, D. A. *Biophys. J.* **1980**, *10*, 515–529.
(30) We follow the convention of Spiess (ref 17) that $|\nu_z| \geq |\nu_x| \geq |\nu_y|$. If $\cos^2\Theta_0 < {}^1/_3$ (i.e., $\Theta_0 > 35.26°$), relabeling the principal axes in Figure 2 makes the averaged principal frequencies follow the above convention. Equations for principal frequencies for arbitrary Θ_0 are available in the literature.[28,29]

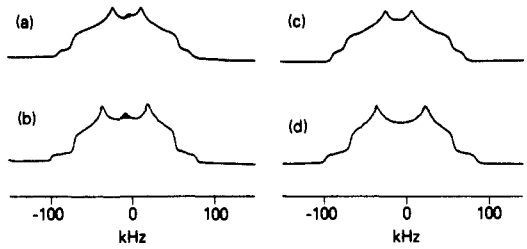

Figure 3. Observed 76.77-MHz quadrupole echo spectra of (a) $^2H_2$-Pro and (b) $^2H_2$-Pro·HCl at 20 °C compared with their respective spectra, c and d, calculated assuming a fast-limit powder pattern having the values of ν_Q and $\bar{\nu}_s$ listed in Table I. Note that all 76.77-MHz spectra have a small intensity artifact at the carrier frequency. This artifact is shaded in this and in subsequent figures.

If $\Theta_0 \leq 35.26°$, the three averaged principal frequencies $\bar{\nu}_x$, $\bar{\nu}_y$, $\bar{\nu}_z$ satisfy the following equations:

$$\nu_Q = 2|\bar{\nu}_x| = 2|\nu_x| \tag{4}$$

$$\bar{\nu}_Q = \bar{\nu}_z = \nu_Q(3\cos^2\Theta_0 - 1)/2 \tag{5}$$

$$\bar{\nu}_s = 2|\bar{\nu}_y| = \nu_Q(1 - 3\sin^2\Theta_0) \tag{6}$$

$$\bar{\eta} = (\bar{\nu}_y - \bar{\nu}_x)/\bar{\nu}_z = \nu_Q/\bar{\nu}_Q - 1 \tag{7}$$

If the two orientations of the carbon–deuterium bond axis have different equilibrium populations, p_1 and p_2, eq 4 remains valid, and if $\Theta_0 \leq 35.26°$, the expression for $\bar{\nu}_s$ becomes

$$\bar{\nu}_s = 2|\bar{\nu}_y| = (\nu_Q/2)(3\sqrt{1 - 4p_1p_2\sin^2 2\Theta_0} - 1) \tag{8}$$

The expression for $\bar{\nu}_z$ is readily obtained from eq 4 and 8 since the sum of the principal frequencies is 0. It should be noted that, when p_1 equals p_2, the x principal axis is as shown in Figure 2, but the z principal axis no longer bisects the angle made by μ_1 and μ_2.

In addition to affecting the ^2H line shape, rapid reorientation also causes spin–lattice relaxation. In the case of two-site exchange, with equilibrium populations p_1 and p_2 the relaxation rate is given by[19]

$$1/T_1 = \omega_Q^2\tau_e p_1p_2\sin^2 2\Theta_0(1 + 3\sin^2\theta\cos^2\phi) \tag{9}$$

Equation 9 is valid when the extreme narrowing condition, $(\omega_0\tau_e)^2 \ll 1$, is satisfied, where ω_0 is the Larmor precession frequency and τ_e equals $1/(k_{12} + k_{21})$. When p_1 equals p_2, $k_{12} = k_{21} = k$ and $\tau_e = 1/(2k)$. The expression for $1/T_1$ for arbitrary values of τ_e is given in ref 19.

An alternative model for reorientation of the carbon–deuterium bond axis is the restricted free diffusion model. In this model the vector representing the bond axis is assumed to reorient in the yz plane, Figure 2. The equilibrium probability of finding $\hat{\mu}$ is constant for Θ less than or equal to Θ_D and is 0 for Θ greater than Θ_D. In the fast-motion limit, $\omega_Q\tau_D \ll 1$, the orientation of the averaged principal axis system is as shown in Figure 2 (provided that $\Theta_D < 67.5°$) and the averaged quadrupole splitting is given by

$$\nu_s = \nu_Q(3\sin(2\Theta_D)/2\Theta_D - 1)/2 \tag{10}$$

In the extreme narrowing limit, $(\omega_0\tau_D)^2 \ll 1$, the expression for $1/T_1$ is given by[31]

$$1/T_1 = \omega_Q^2\tau_D S\Theta_{rms}^2(1 + 3\sin^2\theta\cos^2\phi) \tag{11}$$

where

$$S = 0.5\sum_{n=1}^{\infty}\frac{\cos^2(2\Theta_D)(1 - (-)^n) + \sin^2(2\Theta_D)(1 + (-)^n)}{n^2(X^2 - n^2)^2} \tag{12}$$

In these equations, $\tau_D = 4\Theta_D^2/\pi D$, $X = 4\Theta_D/\pi$, and D is the rotational diffusion constant.

(31) Wittebort, R. J.; Szabo, A. *J. Chem. Phys.* **1978**, *69*, 1722–1736.

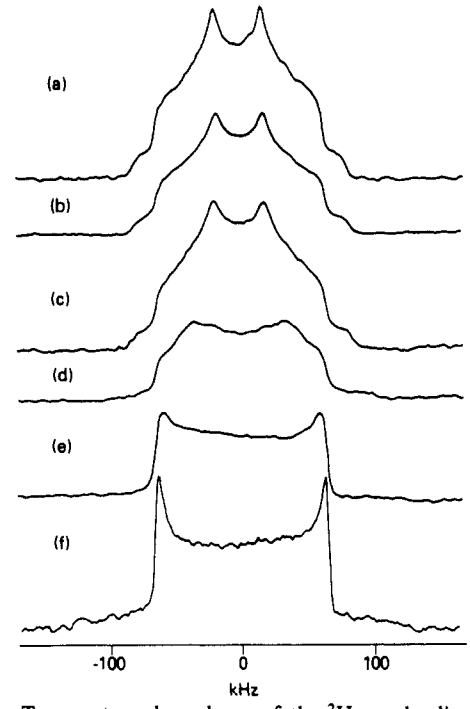

Figure 4. Temperature dependence of the ^2H powder line shape of $^2H_2$-Pro measured at 38.45 MHz by using a quadrupole echo pulse sequence: (a) 49, (b) −35, (c) −85, (d) −130, (e) −156, and (f) −170 °C.

Table I. Temperature Dependence of ν_Q, $\bar{\nu}_s$, $\bar{\nu}_Q$, and Θ_0 for $^2H_2$-Pro and $^2H_2$-Pro·HCl[a]

T, °C	ν_Q, kHz	$\bar{\nu}_s$, kHz	$\bar{\nu}_Q$, kHz	Θ_0,[b] deg	Θ_0,[c] deg
		$^2H_2$-Pro			
49	125.3	35.7	80.8	29.2	29.1
20	126.6	35.5	81.5	29.3	29.2
−10	127.5	36.0	82.1	29.3	29.2
−35	127.6	35.5	82.3	29.4	29.1
−85	127.3	37.7	82.9	29.0	28.8
−115	129.0	50.3	90.5	26.8	26.5
−130	129.3	79.1	101.4	21.1	22.4
−156	130.0	117.9		10.1	
−170	128.0	128.0	128.0		
		$^2H_2$-Pro·HCl			
20	122.8	58.1	90.6	24.8	24.7
−35	124.5	60.1	92.8	24.5	24.3
−130	128.1	64.8	95.3	24.0	24.4

[a] Maximum uncertainty in frequency measurements ±2%, except ±5% for $^2H_2$-Pro when T = −85 °C. [b] From eq 6. [c] From eq 5.

Results and Discussion

The 76.77-MHz ^2H NMR spectrum of $^2H_2$-Pro, Figure 3a, is an axially asymmetric powder pattern ($\bar{\eta}$ = 0.55) having a quadrupole splitting $\bar{\nu}_s$ of 35.5 kHz. This spectrum departs markedly from the Pake pattern, Figure 1a, expected for a static C–^2H bond. The following evidence shows that the observed pattern results from rapid reorientation of the proline C–^2H bond axes. First, the pattern is temperature sensitive as seen in Figure 4. At −170 °C (the lowest temperature attainable on our spectrometer) the line shape closely approximates a Pake pattern with ν_s = 128 kHz, indicating that motion is responsible for the higher temperature spectra. Second, the spectrum observed at 20 °C is in excellent agreement with the fast-limit (all reorientation rates much greater than ν_Q) spectrum calculated by using the parameters in Table I and shown in Figure 3c. Third, X-ray diffraction studies of crystalline compounds containing proline have shown that the proline ring is often disordered. In the disordered structures the γ carbons have large temperature factors that are thought to result from molecular motion. In particular, crystalline DL-proline hydrochloride has a disordered ring with large temperature factors and $^2H_2$-Pro·HCl exhibits an axially

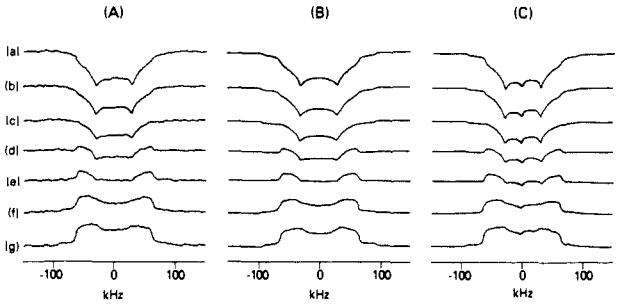

Figure 5. Inversion–recovery quadrupole echo ^2H spectra of $^2H_2$-Pro·HCl measured at −35 °C at two field strengths, (A) 38.45 and (C) 76.77 MHz, compared with (B) spectra calculated by using eq 9, $\Theta_0 = 24.8°$ (see Table I), and τ_e adjusted to give the best-fit value of 0.4 ps. The delay time, t_1, between the π pulse and the first $\pi/2$ pulse was (a) 1.0, (b) 2.0, (c) 4.0, (d) 7.0, (e) 10.0, (f) 15.0, and (g) 20.0 s.

asymmetric powder pattern, Figure 3b, similar to that of $^2H_2$-Pro. Fourth, the frequency (orientation) and the field and temperature dependence of the inverstion–recovery spectra of $^2H_2$-Pro[1] and $^2H_2$-Pro·HCl, Figure 5, are consistent with motion of the proline ring.

The generally accepted model of proline ring motion is one in which various puckered ring conformations interconvert.[5] X-ray diffraction studies have shown that the orientation of proline C–H bond axes in puckered conformations seldom deviate by more than ±35° from their values in the planar ring conformation.[5] Therefore, we take as our initial model of proline ring motion the two-site exchange model, Figure 2, with p_1 equal to p_2 and $\Theta_0 < 35°$. Later we will relax these restrictive assumptions.

We used eq 4–7, together with the measured values of ν_Q, $\bar{\nu}_s$, and $\bar{\nu}_Q$ listed in Table I, to derive values of Θ_0 for $^2H_2$-Pro and $^2H_2$-Pro·HCl. The values of Θ_0 were determined at various temperatures and are tabulated in Table I. An examination of the table shows that the same value of Θ_0 is obtained from the measurement of $\bar{\nu}_s$ or $\bar{\nu}_Q$ and that Θ_0 is constant and equal to 29° from 49 to −85 °C. Below −85 °C, Θ_0 decreases as the temperature is lowered, possibly because lattice contraction restricts the amplitude of the motion of the C^γ–^2H bond axis. Another interesting feature of the spectra obtained below −85 °C is that the powder pattern is broadened at $\bar{\nu}_y$ and $\bar{\nu}_z$ but not at $\bar{\nu}_x$. This result can be explained by assuming that there is a small distribution of Θ_0 values at a given temperature. Equations 5 and 6 show that a ±1° variation in Θ_0, about an average value of 21°, produces a 5-kHz variation in $\bar{\nu}_y$ and $\bar{\nu}_z$. Since $\bar{\nu}_x$ is independent of Θ_0, the spectral edge at this frequency remains well-defined, as observed.

There is no evidence that the spectral features observed below −85 °C result from slow motions. Anisotropy observed in inversion–recovery spectra shows that $(\omega_0\tau_e)^2 \ll 1$ down to at least −130 °C. Also, at no temperature do we observe intensity losses or distortion[32] characteristic of spectra obtained when τ_e is in the range 10^{-4}–10^{-7} s.[21,24,32,34] At −156 °C, for example, the integrated signal intensity was constant as t_2 (the delay between the 90° pulses) varied from 15 to 30 μs.

As seen in Table I, the value of Θ_0 obtained for $^2H_2$-Pro·HCl, 24°, is slightly smaller than that obtained for $^2H_2$-Pro at temperatures above −85 °C. However, unlike $^2H_2$-Pro, the value of Θ_0 for $^2H_2$-Pro·HCl is independent of temperature down to at least −130 °C. Also, at this temperature the $^2H_2$-Pro·HCl spectrum (not shown) has sharp maxima defining $\bar{\nu}_y$ and sharp edges defining $\bar{\nu}_x$ and $\bar{\nu}_z$.

If we remove our restriction that $\Theta_0 < 35°$, we find that identical powder patterns are calculated by using either the values of Θ_0 listed in Table I or their complementary angles, i.e., $90 - \Theta_0$.

(32) Spiess, H. W.; Sillescu, H. *J. Magn. Reson.* **1980**, *42*, 381–389.
(33) Rice, D. M.; Wittebort, R. J.; Griffin, R. G.; Meriovitch, E.; Meinwald, Y.; Freed, J. H.; Scherage, H. A. *J. Am. Chem. Soc.* **1981**, *103*, 7707–7710.
(34) Batchelder, L. S.; Sullivan, C. E.; Jelinski, L. W.; Torchia, D. A. *Proc. Natl. Acad. Sci. U.S.A.* **1982**, *79*, 386–389.

Table II. Temperature Dependence of $^2H_2$-Pro and $^2H_2$-Pro·HCl Correlation Times,[a] τ_e, Obtained by Using Eq 9 to Simulate the Inversion–Recovery Spectra[b]

compd	T, °C	τ_e, ps
$^2H_2$-Pro	49	1.0
	20	1.3
	−11	1.7
	−35	2.0
	−85	3.9
$^2H_2$-Pro·HCl	20	0.3
	−35	0.4
	−130	0.9

[a] Uncertainty ±10%. [b] In eq 9, $\Theta_0 = 29.3°$ and $\nu_Q = 127$ kHz were used for $^2H_2$-Pro, and $\Theta_0 = 24.5°$ and $\nu_Q = 125$ kHz were used for $^2H_2$-Pro·HCl at all temperatures.

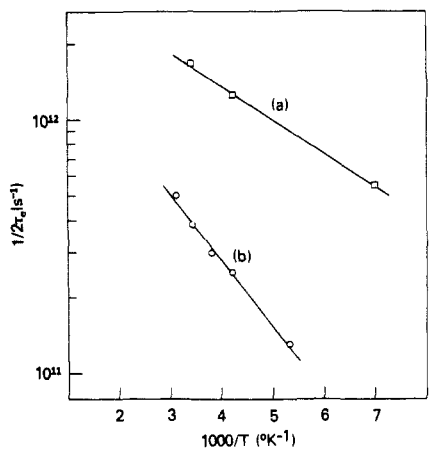

Figure 6. Two-site exchange rate, $1/2\tau_e$, of the C^γ–^2H bond axis plotted against inverse absolute temperature: (a) $^2H_2$-Pro·HCl and (b) $^2H_2$-Pro.

Because the values of Θ_0 never exceed 30° in Table I, this second set of solutions requires that the C^γ–^2H bond axis departs from its planar ring orientation by at least ±60°. Therefore, this set of solutions can be ruled out by (a) the absence of such conformations in crystal structures,[5] (b) the conformational energy calculations,[5] and (c) the fact that $\bar{\nu}$ decreased monotonically from a value of 0.54 to 0 as the temperature of $^2H_2$-Pro dropped from −85 to −170 °C. This observation is consistent with a reduction in Θ_0 from 29°, but not 62°, to 0° in the −85 to −170 °C temperature range.

In addition to providing values of Θ_0, the motionally averaged line shapes also show that the correlation time of the ring motion is less than ca. 10^{-8} s at all temperatures studied. This conclusion follows from the observation of sharp edges and narrow maxima in the spectra and the absence of distorted line shapes and intensity losses which occur when correlation times are in the 10^{-4}–10^{-7}-s range.[21,23,32-34] At 20 °C, for instance, the line shape is unchanged and the intensity decreases by only 10% when t_2 is changed from 20 to 60 μs.

The value of the correlation time was obtained as a function of temperature from analyses of inversion–recovery spectra of $^2H_2$-Pro and $^2H_2$-Pro·HCl. Examination of Figure 5 shows that the spin–lattice relaxation of $^2H_2$-Pro·HCl at 20 °C is (a) frequency (orientation) dependent and (b) independent of field strength. The orientation dependence seen in Figure 5 was observed at all other temperatures for $^2H_2$-Pro·HCl and for $^2H_2$-Pro. The field independence of T_1 shows that τ_e is in the extreme narrowing limit, $(\omega_0\tau_e)^2 \ll 1$. Hence, we can use eq 8 to analyze the inversion–recovery spectra. Note that eq 8 predicts the relaxation time for each frequency component (calculated for each (θ, ϕ) value according to eq 3), and this enables one to calculate inversion–recovery spectra as has been done in Figure 5B. The excellent agreement of the observed and predicted orientation dependence of the inversion–recovery spectra is further evidence that $(\omega_0\tau_e)^2 \ll 1$. The T_1 anisotropy calculated with the assumption that τ_e is outside the extreme narrowing limit disagrees with the observed results. Because both Θ_0 and ν_Q were known,

Table III. Values of ν_Q, $\bar{\nu}_s$,[a] and Θ_0[b] for the β, γ, and δ Deuterons of $^2H_6$-Pro and $^2H_6$-Pro·HCl[c]

compd	T, °C	ν_Q, kHz	$\bar{\nu}_s(\beta)$, kHz	$\bar{\nu}_s(\gamma)$, kHz	$\bar{\nu}_s(\delta)$, kHz	$\Theta_0(\beta)$, deg	$\Theta_0(\gamma)$, deg	$\Theta_0(\delta)$, deg
$^2H_6$-Pro	20	127.3 118.4[c]	73.4	37.7	106.0	22.1	29.0	10.8
	−35	128.1 120.6[c]	75.7	38.2	108.5	21.7	28.9	10.5
$^2H_6$-Pro·HCl	20	122.8	76.5	57.2	102.3	20.8	25.0	13.6

[a] Maximum uncertainty in frequency measurements ±2%. [b] From eq 6. [c] δ deuterons, uncertainty ±3 kHz.

as a consequence of the line-shape analysis, the only adjustable parameter used in calculating the spectra in Figure 5B was τ_e. Inversion–recovery spectra were obtained at several temperatures for both $^2H_2$-Pro and $^2H_2$-Pro·HCl, and τ_e was determined at each temperature in the same manner as in Figure 5. The values of τ_e for each sample are tabulated in Table II, and $1/2\tau_e$, the two-site exchange rate, is plotted against $1000/T$ in Figure 6. In Table II it is seen that the correlation times are indeed very small at all temperatures measured for both compounds. Although τ_e was difficult to determine precisely for $^2H_2$-Pro at temperatures below −85 °C, because of the spectral broadening discussed earlier, the τ_e values obtained at −130 and −156 °C were within ±25% of the values obtained by extrapolating the straight line in Figure 6b.

The small correlation times found for $^2H_2$-Pro and $^2H_2$-Pro·HCl indicate that the activation energy for the ring motion is small. This conclusion is confirmed by the plots of the two-site exchange rate ($1/2\tau_e$) against temperature shown in Figure 6. The apparent activation energies obtained from these plots are 1.3 and 0.6 kcal/mol for $^2H_2$-Pro and $^2H_2$-Pro·HCl, respectively.

In view of these small activation energies it is pertinent to ask if meaningful values of Θ_0 and τ_e were derived from our two-site analysis, because a two-site jump model is an appropriate idealization when activation energies are large. We think that our analysis is valid because we have previously shown[23,35] that derived values of Θ_{rms} and τ are independent of the assumed motional model when reorientation about an axis is fast ($\omega_Q\tau \ll 1$) and of small amplitude, $\Theta_{rms} \ll 1$.

We checked the model dependence of our results by repeating the analysis of our data with the restricted free diffusion model of motion. In order to compare the results from the two different models we must calculate the root mean square angular displacement, Θ_{rms}, for each model. It is easy to show that Θ_{rms} is equal to Θ_0 for the jump model and equals $\Theta_D/3^{1/2}$ for the restricted diffusion model. Using the principal frequencies listed in Table I in eq 10, one calculates values of Θ_{rms} for the restricted diffusion model which agree, within 5%, with those obtained from the jump model. The reason for the close agreement between the two models can be seen by writing the series expansions of the trigonometric functions in eq 6 and 10. When this is done one finds that the two models yield the same expressions for $\bar{\nu}_s$ as Θ_{rms} approaches 0.

Turning to the analysis of the inversion–recovery spectra, we note the close similarity between eq 9 and 11. In particular, the angular dependence of $1/T_1$ is identical for the jump and diffusion models. Furthermore, $S\Theta_{rms}^2$ approaches 0.25 $\sin^2 2\Theta_{rms}$ as Θ_{rms} approaches 0. Therefore, the jump and diffusion expressions for $1/T_1$ are identical in the limit of small angle fluctuations. For $\Theta_{rms} < 30°$, the correlation times obtained from the two models, τ_e and τ_D, differ by less than 20%.

Although the insensitivity of the ^2H NMR line shapes and relaxation rates to the equilibrium orientational probability distribution means that analysis of the NMR experiments cannot yield a unique model of proline ring motion, the analysis does provide important model-insensitive parameters: Θ_{rms}, τ, and the apparent activation energy. The fact that the two simple, but extreme, models considered herein give essentially identical values for these parameters means that the values of Θ_{rms}, τ, and ΔF obtained by using a complex, but more realistic, model such as diffusion over a barrier (from one conformational energy minimum to another) will be essentially the same as those obtained by using the simple models considered above. It should be noted that Θ_{rms} decreases as the barrier between two low-energy conformations decreases because the probability of finding the carbon–deuterium bond axis near its mean value increases. This observation provides a simple explanation for our result that both Θ_{rms} and ΔF are smaller for $^2H_2$-Pro·HCl then for $^2H_2$-Pro.

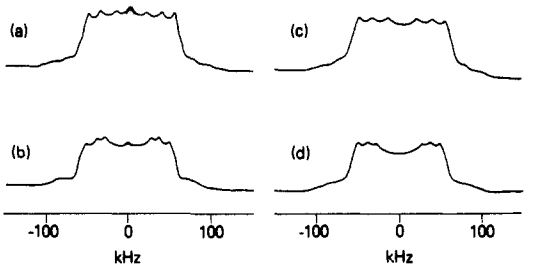

Figure 7. Observed 76.77-MHz ^2H quadrupole echo spectra of (a) $^2H_6$-Pro and (b) $^2H_6$-Pro·HCl at 20 °C compared with their respective spectra, c and d, calculated assuming a fast-limit powder pattern having values of ν_Q and $\bar{\nu}_s$ listed in Table III.

The one common feature of the jump and diffusion models considered thus far is that the equilibrium orientational probability function is symmetrical about the z axis, Figure 2. In the jump model this restriction is removed by assigning different relative populations, p_1 and p_2, to the two orientations of the C^γ–^2H bond axis. In this case Θ_{rms}^2 equals $4p_1p_2\Theta_0^2$, and eq 8 and 9 are used to analyze the line shape and inversion–recovery data. When this is done, again with the assumption that Θ_0 is <35.26°, the values of Θ_{rms} and τ_e are virtually indistinguishable from the values obtained by assuming equal populations at the two sites.

Although we have considered unequal site populations as a possibility, we think that the temperature independence of $\bar{\nu}_s$ observed above −85 °C for $^2H_2$-Pro, and from −130 to 20 °C for $^2H_2$-Pro·HCl, is strong evidence that the low-energy ring conformations have equal populations in these temperature ranges. If this were not so, one would have to explain why the relative populations (a) do not change as the temperature is varied or (b) change in such a way as to keep $\bar{\nu}_s$ constant. Recall, however, that for $^2H_2$-Pro below −85 °C, $\bar{\nu}_s$ does show a monotonic increase as temperature decreases and equals ν_Q at −170 °C. This observation suggests that one of the low-energy conformations is destabilized by contraction of the crystalline lattice at temperatures below −85 °C. Equation 8 shows that $\bar{\nu}_s$ increases and approaches ν_Q as p_1 (or p_2) approaches 0.

In addition to the studies of $^2H_2$-Pro and $^2H_2$-Pro·HCl, we also measured spectra and relaxation times of $^2H_6$-Pro and $^2H_6$-Pro·HCl. Spectra of both compounds are compared with computer simulations in Figure 7. As expected, each compound shows three sets of quadrupole splittings, and the measured values of $\bar{\nu}_s$ are given in Table III. For each compound, the smallest value of $\bar{\nu}_s$ was equal to the value of $\bar{\nu}_s$ observed in the corresponding γ-labeled molecule and was therefore assigned to the γ deuterons. The crystal structure of Pro·HCl shows that the δ carbon has a slightly smaller out-of-plane vibrational amplitude then the β carbon. For this reason and because many studies in solution have shown C^δ to be the least mobile ring carbon, the largest value of $\bar{\nu}_s$ for $^2H_6$-Pro and $^2H_6$-Pro·HCl was assigned to the δ deuterons. By process of elimination the intermediate value of $\bar{\nu}_s$ was then assigned to the β deuterons. The value of Θ_0 was calculated for each ring position by using eq 6 and is listed in Table III. As

(35) Sarkar, S. K.; Sullivan, C. E.; Torchia, D. A. *Biochemistry* **1985**, *24*, 2348–2354.

is evident from the values of Θ_0 listed in the table, the amplitude of the motion at the β and γ positions is substantially larger than that at the δ position.

Inversion-recovery spectra of $^2H_6$-Pro, observed at 20 °C, were in good agreement with spectra calculated by using eq 9 together with the values of Θ_0 and ν_Q for each ring position, Table III, measured from the $^2H_6$-Pro line shape. The same correlation time, 1.1 ps, was used for all three ring positions to calculate the inversion-recovery spectra and was in close agreement with the correlation time observed for $^2H_2$-Pro, Table II. The correlation time obtained for $^2H_6$-Pro·HCl, 0.3 ps, is also in agreement with that listed for $^2H_2$-Pro·HCl in Table II. It is noteworthy that, in spite of the large T_1 values predicted and observed for the hydrochloride compounds, spin diffusion did not cause the angular dependence of T_1 to deviate significantly from that predicted by eq 9.

It is interesting to compare the values of Θ_0 in Table III with the values of Θ_0 obtained from London's analysis[16] of proline ^{13}C NT_1 values measured for peptides in solution. From London's Table I, one finds that Θ_0 is ca. 25° for β and γ positions and is about half as large for the δ position.[36] These results are in close agreement with results in Table III, especially when one considers the obvious difference in ring environments in the two cases. The similarity in Θ_0 values probably arises for the following reasons: First, the peptide nitrogen and α carbon are nearly immobilized by hydrogen bonds in the crystal; in solution these atoms have highly restricted internal motions because they are part of the peptide backbone. Second, the proline ring in the crystal structure[7] resides in a hydrophobic layer which evidently allows as much motional freedom as exists in solution.

In London's analysis,[16] the correlation time for the ring motion was not obtained since analysis of solution relaxation parameters yields the order parameter (amplitude) but not the rate of a very fast internal motion.[37] London did find that $\tau_e < 10^{-10}$ s was required to fit the relaxation data in solution. This result is fully in agreement with the results found herein.

The crystal structure of DL-Pro·HCl shows that the proline ring has an unusual average structure in which the ring is puckered (exo) at the α carbon with the four remaining ring atoms nearly coplanar. In addition the principal axes of the thermal ellipsoids suggest that the β, γ, and δ carbons undergo large amplitude motions in a direction perpendicular to the average plane formed by the nitrogen-C(3)-C(4)-C(5) atoms.

The NMR data show that the large thermal factors do indeed result from such motions rather than from a static statistical distribution of ring structures. Because of the unusual ring puckering and the difference in motional amplitude of the β and δ carbons, it is difficult to describe the ring motion in terms of a simple model. However, it may be possible to simulate the complex motion of the proline ring by means of a molecular mechanics calculation.[38] Indeed, DL-Pro·HCl is an ideal test case for such calculations because its crystal structure is known, and the motions involved are on the picosecond time scale.

A survey of over 50 crystal structures of imino acid and peptide derivatives of proline[5] has shown that the observed ring conformations are consistent with torsional potentials about single bonds. The particular ring conformations found in a specific case are usually determined by packing constraints within the crystal lattice. In the case of DL-proline and its hydrochloride, the proline rings appear to have about as much freedom to move as in solution. The exception to this statement occurs below -85 °C, for $^2H_2$-Pro, where we have suggested that contraction of the crystalline lattice restricts the amplitude of the ring motion. Contraction of the myoglobin unit cell volume has been observed at low temperature.[39] Measurements of the crystal structure of $^2H_2$-Pro in the -80 to -180 °C temperature range would be most interesting, because one could correlate the observed changes in ring dynamics with changes in intermolecular interactions and packing. The different dynamic behavior of the two proline rings in crystalline *cyclo*-(Gly-Pro-D-Ala)$_2$ has demonstrated the sensitivity of proline ring dynamics to molecular environment.[9]

The sensitivity of proline ring dynamics to intermolecular interactions suggests that proline relaxation measurements should be a useful probe of molecular packing within proteins. Such experiments will require enrichment with labeled proline residues but should be worth the effort since they have the potential to provide information about the fluidity of the protein interior in the neighborhood of each proline ring. In addition, one can monitor the influence of interesting variables such as pressure, ligand binding, and temperature on the proline ring environment.

Acknowledgment. We have benefited from helpful discussions with Dr. Attila Szabo, and we thank C. E. Sullivan and R. G. Tschudin for expert technical support.

(36) The equation relating Θ_0 to London's[16] angles β and θ is $\cos 2\Theta_0 = \cos^2\beta + \sin^2\beta \cos 2\theta$.

(37) Lipari, G.; Szabo, A. *J. Am. Chem. Soc.* **1982**, *104*, 4546-4559.

(38) Karplus, M.; McCammon, J. A. *CRC Crit. Rev. Biochem.* **1981**, *9*, 293-349.

(39) Petsko, G. A.; Ringe, D. *Annu. Rev. Biophys. Bioeng.* **1984**, *13*, 331-371.

Low-Temperature Carbon-13 Magnetic Resonance in Solids. 7. Methyl Carbons†

Mark S. Solum, Julio C. Facelli, Josef Michl, and David M. Grant*

Contribution from the Department of Chemistry, University of Utah, Salt Lake City, Utah 84112. *Received February 18, 1986*

Abstract: The principal values of the ^{13}C shielding tensors for a variety of methyl groups in small organic molecules are reported at 25 K. They were measured on neat samples of natural abundance materials. The assignment of the experimental principal values of the shielding tensors to the molecular frame was based on ab initio IGLO (Individual Gauge for Localized Orbitals) calculations of the shielding tensor for cases not determined by symmetry. The analysis of the IGLO bond contributions in the local bond frame was used to obtain some insight into the origin of the chemical shielding and, particularly, of the small variation of the σ_{33} component from compound to compound.

I. Introduction

Recently the use of low-temperature ^{13}C NMR spectroscopy combined with quantum mechanical calculations has been found very useful in the assignment of chemical shielding tensor components with the attendant elucidation of electronic structural features important in nuclear shielding in small organic molecules. Previous work from this laboratory reported the ^{13}C shielding tensors of methylene carbons in a large variety of compounds,[1]

† Part 6 of this series: ref 2.

0002-7863/86/1508-6464$01.50/0